

Reassessing Alkyne Coupling Reactions While Studying the Electronic Properties of Diverse Pyrene Linkages at Surfaces

James Lawrence,* Mohammed S. G. Mohammed, Dulce Rey, Fernando Aguilar-Galindo, Alejandro Berdonces-Layunta, Diego Peña,* and Dimas G. de Oteyza*



Cite This: *ACS Nano* 2021, 15, 4937–4946



Read Online

ACCESS |



Metrics & More



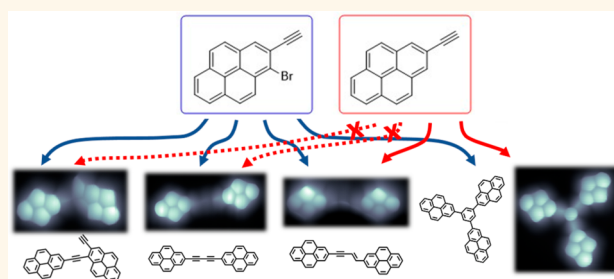
Article Recommendations



Supporting Information

ABSTRACT: The combination of alkyne and halogen functional groups in the same molecule allows for the possibility of many different reactions when utilized in on-surface synthesis. Here, we use a pyrene-based precursor with both functionalities to examine the preferential reaction pathway when it is heated on an Au(111) surface. Using high-resolution bond-resolving scanning tunneling microscopy, we identify multiple stable intermediates along the prevailing reaction pathway that initiate with a clearly dominant Glaser coupling, together with a multitude of other side products. Importantly, control experiments with reactants lacking the halogen functionalization reveal the Glaser coupling to be absent and instead show the prevalence of non-dehydrogenative head-to-head alkyne coupling. We perform scanning tunneling spectroscopy on a rich variety of the product structures obtained in these experiments, providing key insights into the strong dependence of their HOMO–LUMO gaps on the nature of the intramolecular coupling. A clear trend is found of a decreasing gap that is correlated with the conversion of triple bonds to double bonds *via* hydrogenation and to higher levels of cyclization, particularly with nonbenzenoid product structures. We rationalize each of the studied cases.

KEYWORDS: on-surface synthesis, alkyne coupling reactions, conjugation, HOMO–LUMO gap, scanning probe microscopy



INTRODUCTION

On-surface synthesis has been a hot topic in the past 15 years,^{1–8} with a particular focus on forming functional or interesting molecular materials with attractive properties. Often such materials are inaccessible to solution-based synthetic methods, and experimental methods taken from surface science enable researchers to gain detailed insights into their structures and electronic properties. In particular, high-resolution bond-resolving scanning probe microscopies (BR-SPMs) with functionalized tips allow the direct imaging of the chemical structures of as-synthesized species on surfaces.^{9–12} In conventional organic synthesis, the analysis of complex reaction mixtures is often particularly difficult. These mixtures can be formed due to a competition that exists between several different reaction pathways. However, the formation of such mixtures *via* on-surface reactions is not only a problem but also an opportunity. Each product can be identified with BR-SPM, after which scanning tunneling microscopy and spectroscopy (STM/STS) measurements can be used to separately characterize the electronic structure of these species. Under ultrahigh-vacuum conditions, reaction intermediates may also

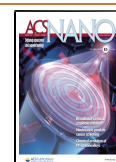
sometimes be generated and observed,¹³ providing insights into possible reaction schemes.

One particular subset of on-surface organic reactions that has attracted considerable attention are those involving alkyne functional groups.¹⁴ Several reactions exist that involve homocoupling to other alkynes, as well as mechanisms that include heterocoupling to different functional groups, such as cycloadditions with azides^{15,16} or couplings with halogenated species.^{17–21} Focusing on alkyne homocoupling, there is already a wide variety of possible reaction schemes that include dehydrogenative Glaser coupling, as well as non-dehydrogenative head-to-head or head-to-tail alkyne coupling, all of which have been readily reported as occurring on coinage metal surfaces under ultrahigh vacuum.^{20,22–30} The two former

Received: November 20, 2020

Accepted: February 22, 2021

Published: February 25, 2021



coupling motifs are difficult to discern,^{22,23} and although most of these works reported Glaser coupling as dominant, the few studies performed with BR-SPM revealed Glaser coupling to be absent and the non-dehydrogenative alkyne coupling to be the most common instead.^{13,25} Nevertheless, it has been recently demonstrated with BR-SPM that on-surface Glaser coupling can occur at the intramolecular level upon tip-induced manipulation.³¹

Focusing now on cross-coupling reactions, Sonogashira coupling involves the formation of a covalent bond between a terminal alkyne and a carbon atom that is initially bound to a halogen atom. Although this reaction is often useful in solution-based synthesis, the on-surface version is less well-studied and more difficult to control,^{18–21} since the starting materials with alkyne and C–X groups can also undergo alkyne or Ullmann coupling reactions, rendering higher levels of selectivity difficult. However, it has been shown that such systems can be controlled kinetically to lead to the desired Sonogashira product,²⁰ as well as *via* the use of templating.²¹

Alkyne groups may also undergo on-surface cyclization reactions such as the Bergman cyclization.^{28,32–34} Cycloaddition reactions, such as the $[2 + 2 + 2]$ ^{22,35–37} and $[1 + 1 + 1]$ ³⁸ types are another possible route toward generating conjugated cyclic linkages. Other varieties such as cascade-type cyclization reactions^{12,39} have also been studied and allow the formation of polymers after the cyclization step. Altogether, the combination of alkyne and halogen groups provides an extremely wide range of possible reaction schemes.

Here, we have chosen a pyrene-based moiety that possesses both a terminal alkyne and a halogen group, potentially allowing for a variety of different homocoupling (Ullmann coupling and alkyne coupling) and cross-coupling (Sonogashira coupling) reaction pathways. However, we anticipate that Ullmann coupling is heavily disfavored by steric hindrance while the planar molecular units are adsorbed on the surface, leaving the less studied Sonogashira and alkyne couplings as the clearly favored options. These basic pathways are summarized in Scheme 1. Furthermore, the vicinal position of the functional groups facilitates an assortment of cyclization reactions that can follow the initial intermolecular coupling. While we find that there is one favored reaction pathway that

begins with Glaser coupling, a multitude of reaction products are found to coexist. The prevalence for an initial Glaser coupling is, however, found to be dependent on the presence of the halogen, since in its absence the non-dehydrogenative head-to-head alkyne coupling is favored instead. The variety of reaction products obtained in these experiments presents an excellent platform for examining the effects of the different coupling motifs on their electronic properties *via* scanning tunneling spectroscopy measurements. Pyrene-based materials are a popular choice for organic electronics,⁴⁰ and quantitatively understanding the effects of changing their coupling allows the more precise design of future materials that can be tailored toward their applications. Importantly, the trends correlating the electronic and structural properties of the bonding motifs are also expected to apply to other organic materials.

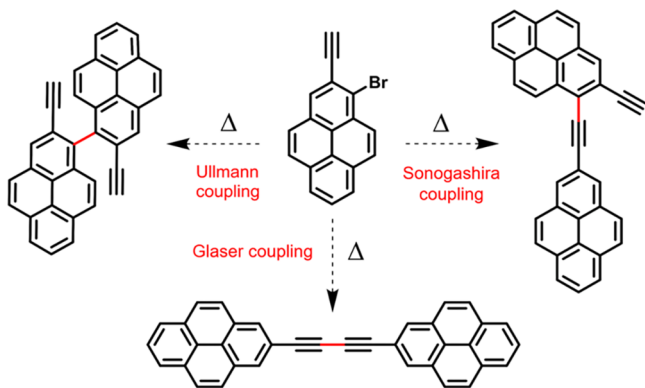
RESULTS AND DISCUSSION

Compound **M1** was prepared by solution chemistry in six steps starting from pyrene, as shown in Figure 1a (see the Supporting Information (SI) for details). First, Ir-catalyzed borylation of pyrene with bis(pinacolato)diboron (B_2pin_2) followed by oxidation of the corresponding $ArB(pin)$ with H_2O_2 led to the formation of pyren-2-ol (**2**). *o*-Bromination of compound **2** with Br_2 and reaction with triflic anhydride (Tf_2O) afforded triflate **3**. Finally, Pd-catalyzed Sonogashira coupling with trimethylsilylacetylene followed by base-induced desilylation led to the formation of 1-bromo-2-ethynylpyrene (**M1**), which was then used as molecular precursor for the on-surface experiments.

As-Deposited Results. The precursor, 1-bromo-2-ethynylpyrene (**M1**, Figure 1a), was sublimed at 358 K onto a room-temperature Au(111) surface. At a low coverage of approximately 0.2 monolayer (ML), most of the molecules self-assemble into dimers, as shown in the STM images in Figure 1b,c. 17% of the molecules are also found alone on the surface, with an even smaller percentage (<4%) showing signs of having lost at least one of their functional groups. As such, it is clear that the C–Br and alkyne groups generally remain intact at room temperature on Au(111), fitting well with many other studies.^{24,37,39,41–44} The self-assembly of **M1**, as well as its susceptibility to tip-induced debromination, is discussed in further detail in the Supporting Information.

Effects of Annealing to 200 and 300 °C. Annealing the same low-coverage sample to 100, 200, and 300 °C yields a variety of molecular structures on the surface. A comparison of the overview STM images obtained after these three annealing temperatures is shown in Figure S3. At 100 °C, many of the molecules are simply debrominated and often self-assemble with one another in a variety of clusters. An example of a BR-STM image of a self-assembled trimer of debrominated precursors (held together by alkyne–alkyne interactions) is shown in Figure S1, next to the pristine molecular dimers for comparison. A further comparison between the imaging of a pyrene with and without the alkyne group is also shown in Figure S4, as well as in Figure S5a–c with BR-STM images. There are some signs of metal–organic structures as well as some covalent bonding occurring at this temperature, but the latter was found to be much more prevalent at higher temperatures. Images and dI/dV spectra of a metal–organic trimer structure are presented in Figure S6. In normal constant current STM imaging, bright features are found between the original position of the Br substituent and the end of the

Scheme 1. Summary of the Three Basic Possible Coupling Reactions That the 1-Bromo-2-ethynylpyrene Precursor May Participate in When Adsorbed on the Au(111) Surface^a



^aNeither the various possible cyclization reactions that may follow nor any trimerization reactions are shown here.

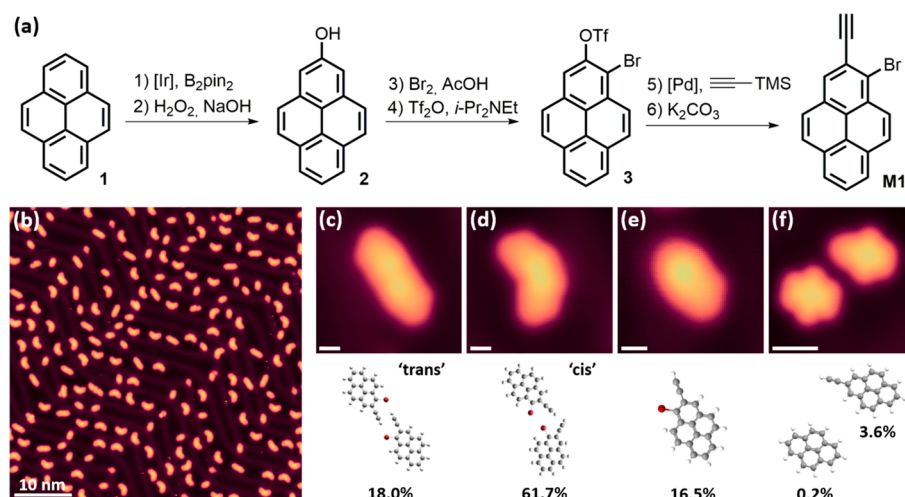


Figure 1. (a) Synthesis of 1-bromo-2-ethynylpyrene (M1). (b) Overview STM image at 4 K ($50 \times 50 \text{ nm}^2$, 30 pA, -1.5 V) of the as-deposited molecule on Au(111). Zoomed in STM images of (c) a trans-type dimer, (d) a cis-type dimer, (e) a lone monomer, and (f) monomers that are missing functional groups. Scale bars are 500 pm. Corresponding optimized models (freestanding) of the two types of self-assembled dimers are shown below their images. The structures of the monomers in panels e and f are also shown for reference. The abundance of each species is also presented alongside the models.

alkyne group, implying two metal–carbon bonds: one between the debrominated pyrene sp^2 carbon and the metal, and another between the same metal atom and the presumably dehydrogenated alkyne terminal sp carbon of an adjacent molecule.

It is not always clear whether the molecules in other self-assembled clusters still possess the radical generated by their debromination, but no indications were found in the BR-STM images of any tilting of the molecules toward the surface or metal adatoms. It may be the case that an unknown fraction of the radicals are passivated by hydrogen atoms that are released by a small number of dehydrogenative reactions that may occur at this temperature, as well as hydrogen that may originate from elsewhere in the ultrahigh-vacuum (UHV) chamber, as has been suggested in other studies.^{45,46}

A large-scale STM image of the objects observed after a 200 °C anneal is shown in Figure 2a. Alongside this is a BR-STM image (Figure 2b) and the corresponding chemical structure (Figure 2c) of the most common species observed at this temperature, the Glaser-coupled dimer D1. Many other species are also found, the most common of which are shown with BR-STM images and their corresponding chemical structures in Figure 2d. BR-STM imaging proved itself to be vital in identifying many of these molecules, as their internal structures (especially when fused to a significant extent) were not always apparent from standard STM imaging. These molecules, along with several others, are observed after annealing to both 200 and 300 °C, in different proportions. A full catalogue of the molecules that were identified with BR-STM imaging in this study is presented in Figure S5. Note that, in contrast to the closely related bond-resolving images obtained by noncontact atomic force microscopy (nc-AFM), in which the higher electron density at triple bonds makes them appear with a brighter contrast,^{9,12,47} in the BR-STM images they rather appear as a node in the current signal.²⁵

Product Statistics. When examining the most common products at both 200 and 300 °C (Table 1), it becomes immediately apparent that several of them are related (a more complete list of the regularly observed molecules and their abundances is provided in Tables S1 and S2). For example, the

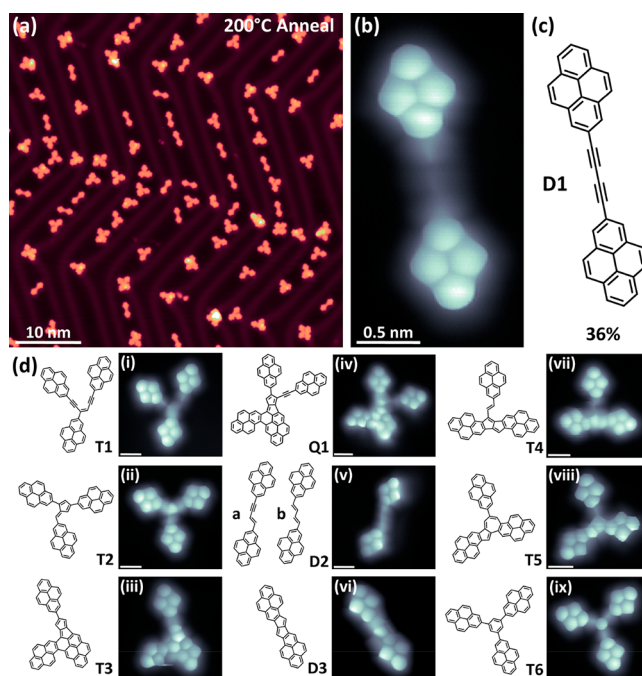
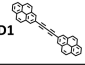
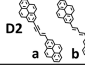
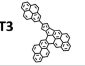
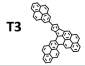
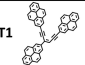
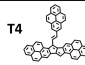
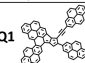
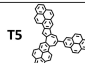


Figure 2. (a) Overview STM image at 4 K ($50 \times 50 \text{ nm}^2$, 55 pA, -1.5 V) of the sample that had been postannealed to 200 °C on Au(111). (b) BR-STM image (CO tip, constant height, 5 mV) of the most common product (Glaser coupling) observed at this annealing temperature. (c) Chemical structure of the Glaser-coupled product D1 with its relative abundance. (d(i–ix)) Various other dimer, trimer, and tetramer structures that are observed, with the corresponding BR-STM images that were used to identify them (CO tip, constant height, 5 mV). Scale bars are all 500 pm.

most common products observed at 200 °C are all part of the reaction path illustrated in Scheme 2: The Glaser-coupled dimer D1 that is most commonly observed can be transformed to trimer T1 upon the addition of a debrominated monomer, forming a *cis*-enediynes in a fashion similar to that of other works.^{23,48} The enediynes fragment of this trimer then cyclizes to form a five-membered ring fulvene moiety (trimer T2,

Table 1. Four Most Common Products for Each Annealing Temperature^a

Most Common Reaction Products					
200 °C Anneal			300 °C Anneal		
Structure	% Molecules	% Pyrenes	Structure	% Molecules	% Pyrenes
	36	27		24	16
	12	13		16	16
	11	12		7	8
	7	10		6	6

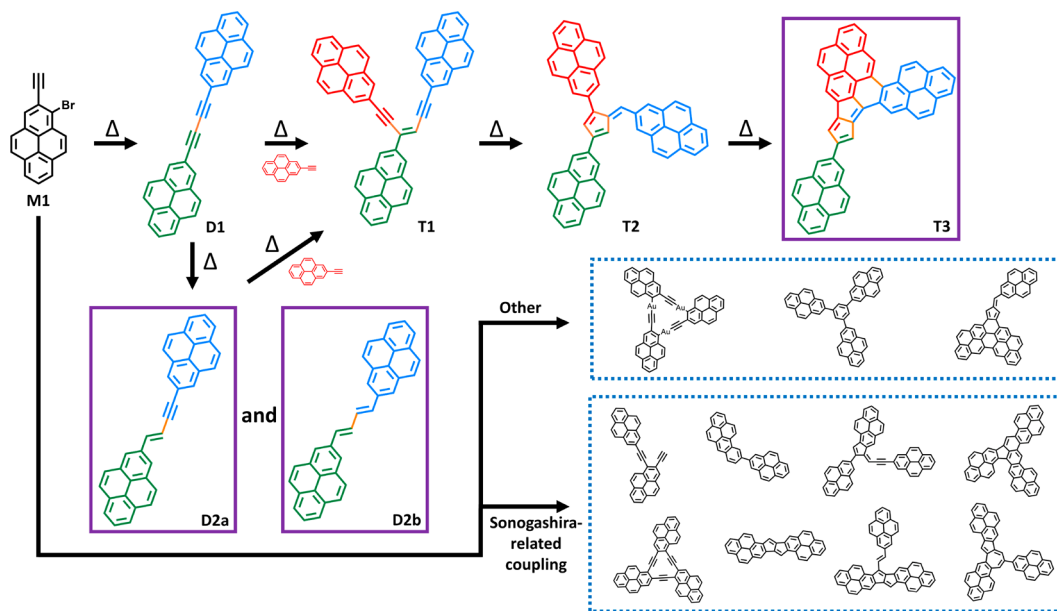
^aEach is presented with the percentage in terms of the total number of molecules, as well as the total number of pyrene components (that is, with different weights for dimers, trimers, and tetramers according to the number of pyrene units or reactant molecules it includes). The two dimers observed at 300 °C have been grouped together as **D2** due to the difficulty found in differentiating them *via* standard STM imaging. The third most common object at 200 °C (**T1**) is essentially no longer found at 300 °C, suggesting that many of them have cyclized to form the most common fused trimer **T3** or other molecules. A total number of 281 molecules (formed by 769 pyrene reactants) have been analyzed for the statistics at 200 °C, whereas 329 molecules (formed by 947 pyrene reactants) have been used for the statistics at 300 °C.

observed less commonly but shown in Figure 2d(ii)). This is an interesting observation, since in solution chemistry the most common cyclization of enediynes is through the Bergman cyclization to obtain a six-membered ring.^{33,49} Thereafter, **T2** can cyclize further to form another five- and six-membered ring, rendering the fused trimer **T3** shown in Figure 2d(iii)

with an integrated pentalene unit that, as will be seen below, has an important influence on the product's electronic properties. The addition of another monomer to **T3** leads to the tetramer **Q1** in Figure 2d(iv). As expected, a subsequent annealing to a higher temperature (300 °C) shifts the observed abundance distribution along the reaction path, decreasing that of the initial intermediates and increasing that of the more advanced product structures such as **T3**. Various possibilities for the reaction mechanisms along this general path are discussed in more detail in the Supporting Information with Figures S7 and S8. The relative concentration of each product after the varying annealing treatments, including that of the intermediates along the main reaction pathway, is known to relate to their respective enthalpies and the various transition states, as well as to molecule-dependent dissipation and entropy.¹³ These issues, however, remain outside of the scope of this work.

The two most common structures observed at 200 °C (**D1**) and 300 °C (**D2**) merely differ in their level of hydrogenation. Whereas **D1** is unambiguously the product of an initial Glaser coupling of **M1**, **D2** could be the result of a non-dehydrogenative head-to-head alkyne coupling of **M1** or from the hydrogenation of **D1**. However, the total absence of **D2** at lower temperatures and its evolution into the most common product at 300 °C, concomitant with an almost complete disappearance of **D1**, make the latter the only plausible scenario. The source of the hydrogen atoms required for this process may be the various other types of dehydrogenative reactions that are occurring elsewhere on the surface at that temperature.

Although the main products of the reactions of **M1** are all related to the initial Glaser-type coupling, many of the other products are in fact related to Sonogashira cross-coupling, as is indicated in the lower part of Scheme 2. Few examples of a

Scheme 2. Most Common Reaction Pathways Found When Annealing 1-Bromo-2-ethynylpyrene on Au(111) to 200 and 300 °C, along with a Variety of Other Products That Are Also Found^a

^aWhile the most abundant products involve an initial Glaser coupling, the formation of several minor products can be associated to an initial Sonogashira coupling (shown here grouped together) and other reaction schemes such as cycloaddition. It is important to note that some of these products are derived from one another.

simple single Sonogashira reaction to form a dimer (for example, molecule **D4** in Figure S5h) are observed, with the case of three molecules forming a cycle (**T7**, Figure S5t) being even more rare. A metal–organic trimer structure that may be a precursor to this was observed after annealing to 100 °C (Figure S6), but the higher quantity of these structures, along with the reversibility of the C–Au bond, may indicate that many of them go on to form other structures at higher annealing temperatures.

Nonetheless, other dimer and trimer structures that are the result of Sonogashira reactions are often observed. Trimer **T5** (Figure 2d(viii)), containing a seven-membered ring, is a relatively common product after annealing to both 200 and 300 °C. Similarly, a fused dimer linked by a pentalene unit (**D3**, Figure 2d(vi)) is the direct result of two Sonogashira-type reactions that may occur simultaneously. This dimer evolves into the trimer **T4** (Figure 2d(vii)) upon the addition of another monomer. Possible reaction mechanisms for both of these are presented in Figures S9 and S10.

It is important to note that there is a significant increase in the number of unusual structures (*i.e.*, structures that were not found regularly) that are observed upon increasing the annealing temperature from 200 to 300 °C. These are counted as “other” in Tables S1 and S2, taking up 19.9% and 32.1% of the pyrenes, respectively. An increase in this number at the higher temperature is not surprising, as an increased number of dehydrogenative couplings and cyclizations are expected, and there are many possible routes that such reactions may take to form a multitude of structures.

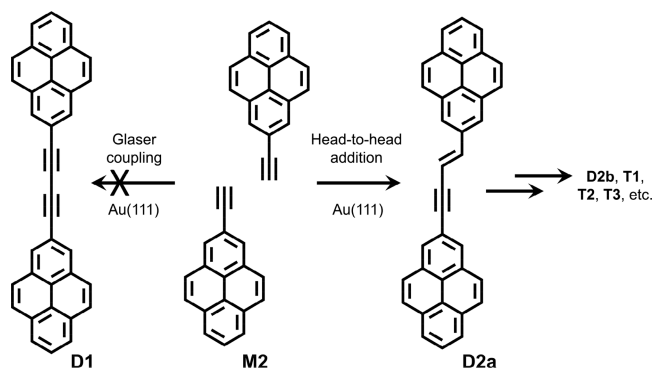
The presented data are obtained from samples with a surface coverage $\theta < 50\%$. Previous works addressing the coverage dependence in precursors undergoing alkyne coupling reactions reported a preference toward dimerization at higher coverage, which in turn switched to a preferred a $[2 + 2 + 2]$ trimerization for $\theta < 50\%$.⁵⁰ Although in these experiments the $[2 + 2 + 2]$ product **T6** (Figure 2d(ix)) is a minority product in spite of the low coverage used, it is worth keeping in mind that the observed ratios may vary for different coverages.

When analyzing the initial reaction at 200 °C, the pronounced favoritism for the Glaser coupling is found to be in striking contrast to the observations with a closely related alkyne-functionalized pyrene (1-ethynylpyrene) on the same substrate, for which a non-dehydrogenative head-to-head addition showed a clear prevalence, as proven by BR-STM.²⁵ A similar dominance of the head-to-head alkyne coupling was also observed on silver by bond-resolving nc-AFM with other organic molecules featuring terminal alkynes.¹³ However, although there are several articles in which it is claimed that Glaser coupling has occurred on a variety of substrates, there are no examples in which BR-SPM has been used to clearly prove the formation of Glaser-coupled products after annealing molecules that only possess terminal alkynes. It may in fact be difficult for typical STM imaging modes to differentiate between the Glaser-coupled product (*e.g.*, **D1** in this study) and the non-dehydrogenative coupling product (*e.g.*, **D2a**) as the structural offset created by its double bond is relatively small when compared to the straight Glaser-coupled dimer. Theoretical calculations modeling the Glaser coupling on silver surfaces indeed show the reaction mechanism to start with an exothermic non-dehydrogenative head-to-head alkyne coupling, followed by an endothermic hydrogen abstraction.²⁹ It thus seems natural to expect the non-dehydrogenative alkyne coupling product to be dominant unless the Glaser coupling

product can be obtained without hydrogen abstraction (*e.g.*, with alkynyl bromides^{27,51}) or the hydrogen abstraction is facilitated (*e.g.*, by nearby halogen atoms).⁵²

Results in the Absence of Halogen atoms. To further investigate this, we have synthesized a 2-ethynylpyrene precursor molecule *without* the ortho-substituted bromine (monomer **M2**, Scheme 3) and deposited it on an Au(111)

Scheme 3. Summary of the Results of Annealing Precursor **M2 on Au(111)^a**



^aWithout a vicinal C–Br group, the Glaser-coupled product **D1** is not formed.

surface with a coverage $\theta < 50\%$. As shown in Figure S11, the as-deposited molecules are clearly identified *via* BR-STM imaging as only possessing their terminal alkyne functional groups, which also direct their self-assembly into trimers at low coverages. Annealing this sample to 100, 200, and 300 °C does *not* yield the Glaser-coupled dimer **D1** at any stage, instead only yielding dimers **D2a** and **D2b** and an assortment of other products (Figure S11c,d). This result is summarized in Scheme 3. It must be noted that, besides the assignment by BR-STM, the various spectroscopic fingerprints discussed below also confirm this conclusion. From the experiments with **M1**, we concluded that the products **D2a** and **D2b** were obtained from the hydrogenation of **D1**. However, this only occurred in a notable amount at the highest tested temperatures (300 °C; see Tables S1 and S2), at which an increasing number of dehydrogenative reaction processes are activated that cause an increase in the atomic hydrogen available on the surface. All of those processes are expected to be the same regardless of whether we have started from **M1** or **M2**, thus discarding that also in the case of **M2** the observed dimers **D2a** and **D2b** are formed by hydrogenation of **D1** readily at low annealing temperatures. Along these lines, it should be remarked that no single dimer **D1** was observed upon annealing **M2** even at the lowest temperatures. It follows that the C–Br group must play a key role in the formation of **D1**, at least on the Au(111) substrate. We presume that the preference for Glaser coupling observed in this work may be promoted by the presence of the vicinal radical that is generated upon dehalogenation. Hydrogen migrations to the radical position (Figure S7) allow the Glaser coupling to occur without a formal loss of hydrogen and the aforementioned associated endothermic effect,²⁹ rendering it thermodynamically more favorable. It may also be the case that any locally coadsorbed atomic bromine favors the Glaser coupling of terminal alkynes, reducing the activation energy by weakening the C–H bond.⁵² Neither of these explanations may be completely discounted without further studies.

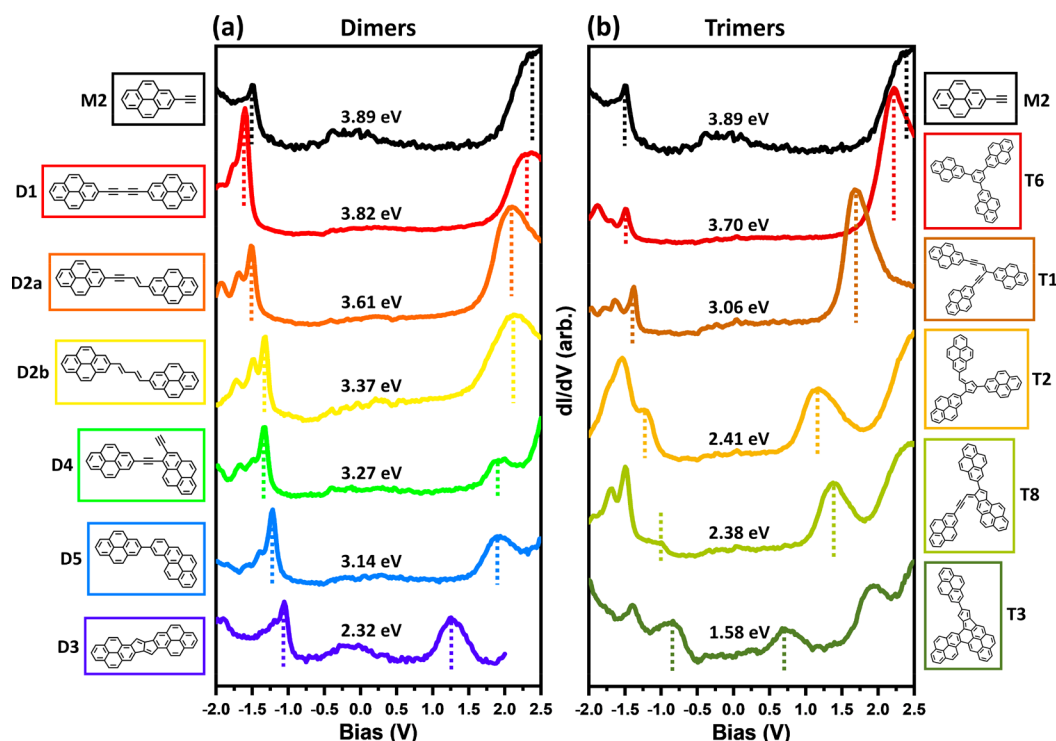


Figure 3. dI/dV point spectra of several different (a) dimers and (b) trimers that were observed after annealing the sample to 200 and 300 °C. The positions at which these spectra were recorded are marked on the BR-STM images in Figures S12 and S13. For each molecule, the highest occupied and lowest unoccupied resonances are marked, with the corresponding HOMO–LUMO gap indicated. A clear shrinking of the HOMO–LUMO gap can be observed when increasing the level of coupling between the pyrene components.

Relationship between the Chemical Structure and the Electronic Structure of the Products. The wide range of products obtained enables a systematic study of the relationship between chemical and electronic structure when considering the different linkages between pyrene moieties. We have thus performed scanning tunneling spectroscopy measurements on several of the molecular species. Differential conductance spectra show clear peaks that correspond to the highest occupied and lowest unoccupied states of the molecules (HOMO and LUMO, respectively), from which the HOMO–LUMO gap has been determined. The measurements obtained on the reference monomer **M2**, as well as on a range of dimers and trimers, are presented in Figure 3, with each category ordered in terms of the measured HOMO–LUMO gap, going from the largest to the smallest. When comparing the types of pyrene coupling to the observed trends in the energy gap, several conclusions can be drawn.

First, the formation of a Glaser-coupled dimer **D1** (Figure 3a, red) does not appear to significantly alter the HOMO–LUMO gap when compared to a 2-ethynylpyrene monomer **M2**, despite a small rigid downshift in the electronic states of the molecule. Since the HOMO–LUMO gap of molecular materials is reduced as the conjugation and the associated electron delocalization increases,⁵³ the formation of a single bond between the alkyne groups does not seem to be a particularly effective channel for conjugation. Changing one of the triple bonds into a double bond (**D2a**, Figure 3a, orange) reduces the energy gap by approximately 0.2 eV. This implies an increased level of conjugation with the double bond in comparison to the triple bond, resulting in a smaller HOMO–LUMO gap. A comparison may be drawn to the difference in energy gap between phenylacetylene and styrene, with a

smaller gap predicted for the latter.⁵⁴ The transformation of the remaining triple bond to a double bond in **D2b** (Figure 3a, yellow) further lowers the energy gap by approximately another 0.2 eV. Imaging the spatial distribution of the frontier electronic states supports the better electronic coupling between the pyrenes in both **D2a** and **D2b**, which both display a notable intensity of the frontier electronic states over the linking conjugated double bond structures (Figure S12). In stark contrast, the equivalent map on the Glaser-coupled dimer **D1** reveals a pronounced and wide node along the linking motif (Figure S12), which can be rationalized as an antibonding scenario of the respective pyrene HOMO orbitals with a consequently weak coupling and very little difference made to the energy gap when compared to the monomer **M2**.

The dimer obtained *via* a Sonogashira reaction has a larger impact on the gap, with a reduction by approximately 0.6 eV relative to the monomer (**D4**, Figure 3a, green). This reveals an increased level of conjugation when directly adding an alkyne group to this position on the pyrene ring, adjacent to the original alkyne group. The dI/dV images of this molecule at the HOMO and LUMO energies, presented in Figure S12, show a clear difference between the two constituent pyrenes, with the majority of the intensities of both HOMO and LUMO (although more prominently the former) found over the pyrene with two alkyne groups attached to it. In molecular structures displaying conjugated segments connected by more poorly conjugated linkages (e.g., with cross-conjugation), their HOMO–LUMO gap is typically determined by the largest of the conjugated segments.^{55,56} Our results can thus be qualitatively understood as a pyrene unit with two conjugated ethynyl groups (their conjugation is further promoted by their ortho positions) that consequently hosts the HOMO and

LUMO and a weaker conjugation to the second pyrene. If the two ethynyl groups cyclize to form the dimer **D5** (Figure 3a, light blue), the same scenario is further enhanced. The new ring is cata-fused, preventing the formation of an additional Clar sextet that would limit the electron delocalization outside the ring. Instead, the conjugation is increased, which is mirrored in a further reduction of the gap. As expected, the HOMO intensity remains mostly localized on the “extended pyrene” (Figure S12).

The largest gap reduction for the dimers, down to 2.32 eV, is obtained in dimer **D3** (Figure 3a, dark blue), in which the two pyrene units are linked by two five-membered rings that make up a pentalene unit. The presence of nonbenzenoid rings in polyaromatic hydrocarbons often leads to low gap values, occasionally even resulting in antiaromaticity or open-shell characters.^{57–59} It is thus not surprising to find **D3** as the lowest HOMO–LUMO gap dimer structure. The efficient electronic coupling between the two pyrenes and the associated electron delocalization is further corroborated by the conductance maps of the HOMO and LUMO, which are both extended over the whole structure and include a strong intensity over the pentalene moiety.

Similar conclusions can be drawn from the analysis of trimer structures. Due to the larger molecular size, one would naively expect lower HOMO–LUMO gap values.⁵³ However, as seen with the dimers, this depends dramatically on the coupling motif. The symmetric $[2 + 2 + 2]$ cycloaddition trimer **T6** in Figure 3b (dark red) has the largest energy gap among the trimers, with a value close to the monomer **M2**/Glaser-coupled dimer **D1**, implying a very small electronic coupling among the different pyrene units. The aromatic ring within the linking motif, not directly coupled to any of the pyrene units, limits the electron delocalization outside the ring.⁶⁰ This can be rationalized when considering the Clar formula of the system, which displays an isolated Clar sextet within the central ring. Any resonant structure with a double bond between the pyrene units and the central ring would be a radical species that displays fewer Clar sextets, with an associated energetic cost.⁶¹ In addition, the three pyrenes are linked to the central aromatic ring at meta positions, causing a cross-conjugation that further limits the electron delocalization.^{25,62,63} Altogether, the three attached pyrenes can almost be pictured as separate isolated “legs”.

Focusing on the *cis*-enediynes trimer **T1** (Figure 3b, light brown), we find a substantially reduced HOMO–LUMO gap of 3.06 eV. In this case the coupling motif is such that while one of the pyrene units is conjugated to the other two, these two are only cross-conjugated with one another. Of the two linear conjugation paths along the coupling motif, one is longer than those discussed earlier, whereas the other is comparable to that discussed with **D2a**. As expected, the additional conjugated path to a third pyrene thus lowers the gap value below that of **D2a**. *dI/dV* imaging of the frontier states in Figure S13 clearly shows a much higher intensity over this linking structure for both the highest occupied and lowest unoccupied states. Fusing the central *cis*-enediynes linkages into a conjugated fulvene structure significantly lowers the energy gap even further, as shown by **T2** with its much smaller energy gap of 2.41 eV. Again, *dI/dV* imaging of this molecule (Figure S13) clearly demonstrates a strong association of the frontier resonances with the nonbenzenoid connecting ring. If the five-membered ring is directly fused to one of the pyrene units (**T8**), the gap is also small, with the conductance maps again

revealing a HOMO that is dominantly localized on the “extended pyrene” (Figure S13).

The lowest HOMO–LUMO gap of all of the products studied is found for trimer **T3** (Figure 3b, dark green), with a value of 1.58 eV. We find the following particularities in this structure: (i) the three pyrenes are conjugated with one another; (ii) two of the pyrenes are in fact fully fused by an aromatic ring, generating a large polycyclic unit; (iii) the bonding motif again includes the antiaromatic pentalene moiety that indeed hosts much of the otherwise fully delocalized HOMO and LUMO signal in conductance maps (Figure S13). Following reasoning similar to that above, all of these contribute to a substantial lowering of the HOMO–LUMO gap and explain its particularly low value.

In order to corroborate our conclusions, we have performed additional density functional theory calculations for the various analyzed structures in a freestanding configuration. The results confirm the same HOMO–LUMO gap trend as found experimentally. Indeed, a fit to the experimentally obtained gaps plotted against the calculated values (Figure S14) provides a nice linear correlation with slope 1.2 and an offset of around -0.34 eV that corresponds to the gap underestimation that is generally obtained in density functional theory (DFT). This excellent agreement, along with the resemblance of the calculated orbitals to the experimentally obtained *dI/dV* maps of the frontier orbitals (shown for each molecule in Figures S12 and S13), provides additional confirmation of our structural assignments of the products, as well as of the conclusions regarding the interrelations between linking structure and electronic properties.

Since we have clearly shown the effect of all of these different linkages, we hope that it can provide a reference for future works, in particular those that aim to synthesize conjugated polymers or nanoribbons that are formed from similar components. Indeed, recent works have shown the critical role that the electronic coupling of different linking motifs have on the band gap of organic polymers, which can be used to design structures with very low band gap values.^{64,65} Controlling these linkages thus allows a precise control of the HOMO–LUMO gap of small molecules, as well as the engineering of polymeric conjugated systems with tunable band gaps.

CONCLUSIONS

We have extensively examined the reaction pathways of a pyrene derivative with vicinal alkyne and bromine substituents on the Au(111) surface. The precursor was found to favor Glaser coupling, followed by the formation of increasingly fused trimer structures at higher temperatures due to different cyclization reactions. However, control experiments using a nonbrominated precursor have clearly demonstrated that the Glaser-coupled product is only formed when there is also a C–Br group attached to the molecule. In its absence, the alkyne coupling reactions show a pronounced favoritism for non-dehydrogenative head-to-head addition. Altogether, a manifold of molecular structures was obtained from these experiments. In the presence of alkyne and halogen groups, many products that resulted from Sonogashira-type coupling were also observed, as well as various intermediates. This wide variety of products has allowed an extensive study of the electronic properties of different linkages between pyrene moieties, with a clear relationships found that link the formation of double bonds, new rings, and antiaromatic pentalene motifs with a

narrower HOMO–LUMO gap. We hope that this knowledge may help to guide the design of extended conjugated systems in the future, such that their band gaps may be more easily controlled according to our needs.

METHODS

All STM and STS measurements were performed with a commercial Omicron-Scienta ultrahigh-vacuum LT-STM instrument at 4.3 K. An Au(111) single crystal (MaTeck) was used as a substrate. The crystal was cleaned *via* cycles of Ar⁺ sputtering and annealing up to 720 K. 1-Bromo-2-ethynylpyrene (**M1**) was sublimed at 85 °C onto the Au(111) substrate while it was held at room temperature. In contrast to this, 2-ethynylpyrene (**M2**) readily sublimed at room temperature and was also deposited onto a room-temperature Au(111) sample. In order to functionalize the tip for BR-STM measurements, CO was postdeposited directly onto the cold sample while it was inside the STM at <7 K by leaking the gas into the chamber to a pressure of approximately 5×10^{-9} mbar. Picking up the CO molecule was usually achieved by scanning at higher currents (approximately 500 pA or higher) and negative voltages (−0.5 to −1.5 V). dI/dV measurements were typically performed with a bias voltage oscillation frequency of 731 Hz and an amplitude of 20 mV.

The syntheses and characterizations of precursor molecules **M1** and **M2** are described in the [Supporting Information](#).

All of the calculations were done in the frame of density functional theory using the Gaussian16 package.⁶⁶ We have employed the M06-2X functional,⁶⁷ which provides good geometries and includes weak interactions (e.g., dispersion forces), with the double- ζ cc-pVDZ basis set.⁶⁸ On the top of the optimized structures, which have been identified as minima through a vibrational analysis, we have performed single point calculations with the same basis and the HSE06 functional,⁶⁹ a hybrid functional that provides good energies for the HOMO–LUMO gap. Structures and molecular orbitals were visualized with GaussView6.⁷⁰

ASSOCIATED CONTENT

Supporting Information

The Supporting Information is available free of charge at <https://pubs.acs.org/doi/10.1021/acsnano.0c09756>.

Description of as-deposited self-assembled structures; evidence of tip-induced debromination events; **M1** sample overview images; images of reactant molecules' missing functional groups; summary of reproducibly observed reaction products and their structural assignment; images and spectroscopic data of metal–organic intermediates; tables reporting the obtained products' statistics; reaction mechanism proposals; **M2** overview and zoom in images; frontier orbital conductance maps for structures analyzed in [Figure 3](#); theory/experiment HOMO–LUMO gaps correlations; synthetic methods and associated NMR spectra ([PDF](#))

AUTHOR INFORMATION

Corresponding Authors

James Lawrence – Donostia International Physics Center, 20018 San Sebastián, Spain; Centro de Física de Materiales, 20018 San Sebastián, Spain; orcid.org/0000-0001-5503-8661; Email: james.lawrence@dipec.org

Diego Peña – Centro Singular de Investigación en Química Biolóxica e Materiais Moleculares (CiQUS) and Departamento de Química Orgánica, Universidade de Santiago de Compostela, 15782 Santiago de Compostela, Spain; orcid.org/0000-0003-3814-589X; Email: diego.pena@usc.es

Dimas G. de Oteyza – Donostia International Physics Center, 20018 San Sebastián, Spain; Centro de Física de Materiales, 20018 San Sebastián, Spain; Ikerbasque, Basque Foundation for Science, 48011 Bilbao, Spain; orcid.org/0000-0001-8060-6819; Email: d_g_oteyza@ehu.es

Authors

Mohammed S. G. Mohammed – Donostia International Physics Center, 20018 San Sebastián, Spain; Centro de Física de Materiales, 20018 San Sebastián, Spain; orcid.org/0000-0002-5544-611X

Dulce Rey – Centro Singular de Investigación en Química Biolóxica e Materiais Moleculares (CiQUS) and Departamento de Química Orgánica, Universidade de Santiago de Compostela, 15782 Santiago de Compostela, Spain

Fernando Aguilar-Galindo – Donostia International Physics Center, 20018 San Sebastián, Spain; orcid.org/0000-0003-2751-5592

Alejandro Berdonces-Layunta – Donostia International Physics Center, 20018 San Sebastián, Spain; Centro de Física de Materiales, 20018 San Sebastián, Spain

Complete contact information is available at:

<https://pubs.acs.org/doi/10.1021/acsnano.0c09756>

Notes

The authors declare no competing financial interest.

ACKNOWLEDGMENTS

We acknowledge funding from the European Union's Horizon 2020 programme (Grant Agreement Nos. 635919 (“SUR-FINK”) and 863098 (“SPRING”)), from the Spanish Agencia Estatal de Investigación (Grant Nos. PID2019-107338RB-C62 and PID2019-107338RB-C63), Xunta de Galicia (Centro singular de investigación de Galicia, 2019–2022, Grant No. ED431G 2019/03), and the European Regional Development Fund-ERDF for financial support. We acknowledge the generous allocation of computer time at the computing center of Donostia International Physics Center.

REFERENCES

- (1) Shen, Q.; Gao, H. Y.; Fuchs, H. Frontiers of On-Surface Synthesis: From Principles to Applications. *Nano Today* **2017**, *13*, 77–96.
- (2) Wang, T.; Zhu, J. Confined On-Surface Organic Synthesis: Strategies and Mechanisms. *Surf. Sci. Rep.* **2019**, *74* (2), 97–140.
- (3) Sun, Q.; Zhang, R.; Qiu, J.; Liu, R.; Xu, W. On-Surface Synthesis of Carbon Nanostructures. *Adv. Mater.* **2018**, *30* (17), 1705630.
- (4) Held, P. A.; Fuchs, H.; Studer, A. Covalent-Bond Formation *via* On-Surface Chemistry. *Chem. - Eur. J.* **2017**, *23* (25), 5874–5892.
- (5) Fan, Q.; Gottfried, J. M.; Zhu, J. Surface-Catalyzed C-C Covalent Coupling Strategies toward the Synthesis of Low-Dimensional Carbon-Based Nanostructures. *Acc. Chem. Res.* **2015**, *48* (8), 2484–2494.
- (6) Dong, L.; Liu, P. N.; Lin, N. Surface-Activated Coupling Reactions Confined on a Surface. *Acc. Chem. Res.* **2015**, *48* (10), 2765–2774.
- (7) Grill, L.; Hecht, S. Covalent On-Surface Polymerization. *Nat. Chem.* **2020**, *12*, 115–130.
- (8) Clair, S.; De Oteyza, D. G. Controlling a Chemical Coupling Reaction on a Surface: Tools and Strategies for On-Surface Synthesis. *Chem. Rev.* **2019**, *119* (7), 4717–4776.
- (9) Jelinek, P. High Resolution SPM Imaging of Organic Molecules with Functionalized Tips. *J. Phys.: Condens. Matter* **2017**, *29* (34), 343002.

- (10) Gross, L.; Schuler, B.; Pavliček, N.; Fatayer, S.; Majzik, Z.; Moll, N.; Peña, D.; Meyer, G. Atomic Force Microscopy for Molecular Structure Elucidation. *Angew. Chem., Int. Ed.* **2018**, *57* (15), 3888–3908.
- (11) Krejčí, O.; Hapala, P.; Ondráček, M.; Jelínek, P. Principles and Simulations of High-Resolution STM Imaging with a Flexible Tip Apex. *Phys. Rev. B: Condens. Matter Mater. Phys.* **2017**, *95*, 045407.
- (12) de Oteyza, D. G.; Gorman, P.; Chen, Y.-C.; Wickenburg, S.; Riss, A.; Mowbray, D. J.; Etkin, G.; Pedramrazi, Z.; Tsai, H.-Z.; Rubio, A.; Crommie, M. F.; Fischer, F. R. Direct Imaging of Covalent Bond Structure in Single-Molecule Chemical Reactions. *Science* **2013**, *340* (6139), 1434–1437.
- (13) Riss, A.; Paz, A. P.; Wickenburg, S.; Tsai, H. Z.; De Oteyza, D. G.; Bradley, A. J.; Ugeda, M. M.; Gorman, P.; Jung, H. S.; Crommie, M. F.; Rubio, A.; Fischer, F. R. Imaging Single-Molecule Reaction Intermediates Stabilized by Surface Dissipation and Entropy. *Nat. Chem.* **2016**, *8* (7), 678–683.
- (14) Klappenberger, F.; Zhang, Y. Q.; Björk, J.; Klyatskaya, S.; Ruben, M.; Barth, J. V. On-Surface Synthesis of Carbon-Based Scaffolds and Nanomaterials Using Terminal Alkynes. *Acc. Chem. Res.* **2015**, *48* (7), 2140–2150.
- (15) Bebensee, F.; Bombis, C.; Vadapoo, S. R.; Cramer, J. R.; Besenbacher, F.; Gothelf, K. V.; Linderoth, T. R. On-Surface Azide-Alkyne Cycloaddition on Cu(111): Does It “Click” in Ultrahigh Vacuum? *J. Am. Chem. Soc.* **2013**, *135* (6), 2136–2139.
- (16) Díaz Arado, O.; Mönig, H.; Wagner, H.; Franke, J. H.; Langewisch, G.; Held, P. A.; Studer, A.; Fuchs, H. On-Surface Azide-Alkyne Cycloaddition on Au(111). *ACS Nano* **2013**, *7* (10), 8509–8515.
- (17) Kanuru, V. K.; Kyriakou, G.; Beaumont, S. K.; Papageorgiou, A. C.; Watson, D. J.; Lambert, R. M. Sonogashira Coupling on an Extended Gold Surface in Vacuo: Reaction of Phenylacetylene with Iodobenzene on Au(111). *J. Am. Chem. Soc.* **2010**, *132* (23), 8081–8086.
- (18) Sánchez-Sánchez, C.; Yubero, F.; González-Elipe, A. R.; Feria, L.; Sanz, J. F.; Lambert, R. M. The Flexible Surface Revisited: Adsorbate-Induced Reconstruction, Homocoupling, and Sonogashira Cross-Coupling on the Au(100) Surface. *J. Phys. Chem. C* **2014**, *118* (22), 11677–11684.
- (19) Sanchez-Sanchez, C.; Orozco, N.; Holgado, J. P.; Beaumont, S. K.; Kyriakou, G.; Watson, D. J.; Gonzalez-Elipe, A. R.; Feria, L.; Fernández Sanz, J.; Lambert, R. M. Sonogashira Cross-Coupling and Homocoupling on a Silver Surface: Chlorobenzene and Phenylacetylene on Ag(100). *J. Am. Chem. Soc.* **2015**, *137* (2), 940–947.
- (20) Wang, T.; Huang, J.; Lv, H.; Fan, Q.; Feng, L.; Tao, Z.; Ju, H.; Wu, X.; Tait, S. L.; Zhu, J. Kinetic Strategies for the Formation of Graphyne Nanowires via Sonogashira Coupling on Ag(111). *J. Am. Chem. Soc.* **2018**, *140* (41), 13421–13428.
- (21) Zhang, R.; Lyu, G.; Li, D. Y.; Liu, P. N.; Lin, N. Template-Controlled Sonogashira Cross-Coupling Reactions on a Au(111) Surface. *Chem. Commun.* **2017**, *53* (10), 1731–1734.
- (22) Gao, H. Y.; Wagner, H.; Zhong, D.; Franke, J. H.; Studer, A.; Fuchs, H. Glaser Coupling at Metal Surfaces. *Angew. Chem., Int. Ed.* **2013**, *52* (14), 4024–4028.
- (23) Gao, H. Y.; Franke, J. H.; Wagner, H.; Zhong, D.; Held, P. A.; Studer, A.; Fuchs, H. Effect of Metal Surfaces in On-Surface Glaser Coupling. *J. Phys. Chem. C* **2013**, *117* (36), 18595–18602.
- (24) Held, P. A.; Gao, H. Y.; Liu, L.; Mück-Lichtenfeld, C.; Timmer, A.; Mönig, H.; Barton, D.; Neugebauer, J.; Fuchs, H.; Studer, A. On-Surface Domino Reactions: Glaser Coupling and Dehydrogenative Coupling of a Biscarboxylic Acid To Form Polymeric Bisacylperoxides. *Angew. Chem., Int. Ed.* **2016**, *55* (33), 9777–9782.
- (25) Mohammed, M. S. G.; Colazzo, L.; Gallardo, A.; Pomposo, J. A.; Jelínek, P.; de Oteyza, D. G. Steering Alkyne Homocoupling with On-Surface Synthesized Metal-Organic Complexes. *Chem. Commun.* **2020**, *56*, 8659–8662.
- (26) Gao, H. Y.; Zhong, D.; Mönig, H.; Wagner, H.; Held, P. A.; Timmer, A.; Studer, A.; Fuchs, H. Photochemical Glaser Coupling at Metal Surfaces. *J. Phys. Chem. C* **2014**, *118* (12), 6272–6277.
- (27) Wang, T.; Lv, H.; Feng, L.; Tao, Z.; Huang, J.; Fan, Q.; Wu, X.; Zhu, J. Unravelling the Mechanism of Glaser Coupling Reaction on Ag(111) and Cu(111) Surfaces: A Case for Halogen Substituted Terminal Alkyne. *J. Phys. Chem. C* **2018**, *122* (26), 14537–14545.
- (28) Wang, T.; Lv, H.; Huang, J.; Shan, H.; Feng, L.; Mao, Y.; Wang, J.; Zhang, W.; Han, D.; Xu, Q.; Du, P.; Zhao, A.; Wu, X.; Tait, S. L.; Zhu, J. Reaction Selectivity of Homochiral versus Heterochiral Intermolecular Reactions of Prochiral Terminal Alkynes on Surfaces. *Nat. Commun.* **2019**, *10*, 4122.
- (29) Björk, J.; Zhang, Y. Q.; Klappenberger, F.; Barth, J. V.; Stafström, S. Unraveling the Mechanism of the Covalent Coupling between Terminal Alkynes on a Noble Metal. *J. Phys. Chem. C* **2014**, *118* (6), 3181–3187.
- (30) Zhang, Y.-Q.; Kepčija, N.; Kleinschrodt, M.; Diller, K.; Fischer, S.; Papageorgiou, A. C.; Allegretti, F.; Björk, J.; Klyatskaya, S.; Klappenberger, F.; Ruben, M.; Barth, J. V. Homo-Coupling of Terminal Alkynes on a Noble Metal Surface. *Nat. Commun.* **2012**, *3*, 1286.
- (31) Albrecht, F.; Rey, D.; Fatayer, S.; Schulz, F.; Pérez, D.; Peña, D.; Gross, L. Intramolecular Coupling of Terminal Alkynes by Atom Manipulation. *Angew. Chem., Int. Ed.* **2020**, *59*, 22989–22993.
- (32) Sun, Q.; Zhang, C.; Li, Z.; Kong, H.; Tan, Q.; Hu, A.; Xu, W. On-Surface Formation of One-Dimensional Polyphenylene through Bergman Cyclization. *J. Am. Chem. Soc.* **2013**, *135* (23), 8448–8451.
- (33) de Oteyza, D. G. Enediyne Cyclization Chemistry on Surfaces Under Ultra-High Vacuum. In *On-Surface Synthesis*; Gourdon, A., Ed.; Springer International; Cham, Switzerland, 2016; pp 85–99, DOI: 10.1007/978-3-319-26600-8_4.
- (34) Schuler, B.; Fatayer, S.; Mohn, F.; Moll, N.; Pavliček, N.; Meyer, G.; Peña, D.; Gross, L. Reversible Bergman Cyclization by Atomic Manipulation. *Nat. Chem.* **2016**, *8* (3), 220–224.
- (35) Zhou, H.; Liu, J.; Du, S.; Zhang, L.; Li, G.; Zhang, Y.; Tang, B. Z.; Gao, H. J. Direct Visualization of Surface-Assisted Two-Dimensional Diyne Polycyclotrimerization. *J. Am. Chem. Soc.* **2014**, *136* (15), 5567–5570.
- (36) Xiang, F.; Lu, Y.; Li, C.; Song, X.; Liu, X.; Wang, Z.; Liu, J.; Dong, M.; Wang, L. Cyclotrimerization-Induced Chiral Supramolecular Structures of 4-Ethynyltriphenylamine on Au(111) Surface. *Chem. - Eur. J.* **2015**, *21* (37), 12978–12983.
- (37) Liu, J.; Ruffieux, P.; Feng, X.; Müllen, K.; Fasel, R. Cyclotrimerization of Arylalkynes on Au(111). *Chem. Commun.* **2014**, *50* (76), 11200–11203.
- (38) Li, Q.; Gao, J.; Li, Y.; Fuentes-Cabrera, M.; Liu, M.; Qiu, X.; Lin, H.; Chi, L.; Pan, M. Self-Assembly Directed One-Step Synthesis of [4]Radialene on Cu(100) Surfaces. *Nat. Commun.* **2018**, *9* (1), 1–7.
- (39) Riss, A.; Wickenburg, S.; Gorman, P.; Tan, L. Z.; Tsai, H. Z.; De Oteyza, D. G.; Chen, Y. C.; Bradley, A. J.; Ugeda, M. M.; Etkin, G.; Louie, S. G.; Fischer, F. R.; Crommie, M. F. Local Electronic and Chemical Structure of Oligo-Acetylene Derivatives Formed through Radical Cyclizations at a Surface. *Nano Lett.* **2014**, *14* (5), 2251–2255.
- (40) Figueira-Duarte, T. M.; Müllen, K. Pyrene-Based Materials for Organic Electronics. *Chem. Rev.* **2011**, *111* (11), 7260–7314.
- (41) Koch, M.; Gille, M.; Viertel, A.; Hecht, S.; Grill, L. Substrate-Controlled Linking of Molecular Building Blocks: Au(111) vs. Cu(111). *Surf. Sci.* **2014**, *627*, 70–74.
- (42) Björk, J.; Hanke, F.; Straßström, S. Mechanisms of Halogen-Based Covalent Self-Assembly on Metal Surfaces. *J. Am. Chem. Soc.* **2013**, *135*, 5768–5775.
- (43) Pham, T. A.; Song, F.; Nguyen, M. T.; Li, Z.; Studener, F.; Stohr, M. Comparing Ullmann Coupling on Noble Metal Surfaces: On-Surface Polymerization of 1,3,6,8-Tetrabromopyrene on Cu(111) and Au(111). *Chem. - Eur. J.* **2016**, *22* (17), 5937–5944.
- (44) Lackinger, M. Surface-Assisted Ullmann Coupling. *Chem. Commun.* **2017**, *53* (56), 7872–7885.
- (45) Talirz, L.; Söde, H.; Cai, J.; Ruffieux, P.; Blankenburg, S.; Jafaar, R.; Berger, R.; Feng, X.; Müllen, K.; Passerone, D.; Fasel, R.;

Pignedoli, C. A. Termini of Bottom-Up Fabricated Graphene Nanoribbons. *J. Am. Chem. Soc.* **2013**, *135* (6), 2060–2063.

(46) Kawai, S.; Takahashi, K.; Ito, S.; Pawlak, R.; Meier, T.; Spijker, P.; Canova, F. F.; Tracey, J.; Nozaki, K.; Foster, A. S.; Meyer, E. Competing Annulene and Radialene Structures in a Single Anti-Aromatic Molecule Studied by High-Resolution Atomic Force Microscopy. *ACS Nano* **2017**, *11* (8), 8122–8130.

(47) Sánchez-Grande, A.; de la Torre, B.; Santos, J.; Cirera, B.; Lauwaet, K.; Chutura, T.; Edalatmanesh, S.; Mutombo, P.; Rosen, J.; Zbořil, R.; Miranda, R.; Björk, J.; Jelínek, P.; Martín, N.; Eciija, D. On-Surface Synthesis of Ethynylene-Bridged Anthracene Polymers. *Angew. Chem., Int. Ed.* **2019**, *58* (20), 6559–6563.

(48) Wang, T.; Lv, H.; Fan, Q.; Feng, L.; Wu, X.; Zhu, J. Highly Selective Synthesis of Cis-Enediyne on a Ag(111) Surface. *Angew. Chem., Int. Ed.* **2017**, *56* (17), 4762–4766.

(49) Prall, M.; Wittkopp, A.; Schreiner, P. R. Can Fulvenes Form from Enediyne? A Systematic High-Level Computational Study on Parent and Benzannelated Enediyne and Enyne-Allene Cyclizations. *J. Phys. Chem. A* **2001**, *105* (40), 9265–9274.

(50) Klaasen, H.; Liu, L.; Meng, X.; Held, P. A.; Gao, H. Y.; Barton, D.; Mück-Lichtenfeld, C.; Neugebauer, J.; Fuchs, H.; Studer, A. Reaction Selectivity in On-Surface Chemistry by Surface Coverage Control—Alkyne Dimerization *versus* Alkyne Trimerization. *Chem. - Eur. J.* **2018**, *24* (57), 15303–15308.

(51) Sun, Q.; Cai, L.; Ma, H.; Yuan, C.; Xu, W. Dehalogenative Homocoupling of Terminal Alkynyl Bromides on Au(111): Incorporation of Acetylenic Scaffolding into Surface Nanostructures. *ACS Nano* **2016**, *10* (7), 7023–7030.

(52) Liu, J.; Chen, Q.; He, Q.; Zhang, Y.; Fu, X.; Wang, Y.; Zhao, D.; Chen, W.; Xu, G. Q.; Wu, K. Bromine Adatom Promoted C-H Bond Activation in Terminal Alkynes at Room Temperature on Ag(111). *Phys. Chem. Chem. Phys.* **2018**, *20* (16), 11081–11088.

(53) Gutzler, R.; Perepichka, D. F. II-Electron Conjugation in Two Dimensions. *J. Am. Chem. Soc.* **2013**, *135* (44), 16585–16594.

(54) Serrano-Andrés, L.; Merchán, M.; Jablonski, M. The Electronic Spectra of Aryl Olefins: A Theoretical Study of Phenylacetylene. *J. Chem. Phys.* **2003**, *119* (8), 4294–4304.

(55) Boldi, A. M.; Anthony, J.; Gramlich, V.; Knobler, C. B.; Boudon, C.; Gisselbrecht, J.-P.; Gross, M.; Diederich, F. Acyclic Tetraethynylethene Molecular Scaffolding: Multinanometer-Sized Linearly Conjugated Rods with the Poly(triacetylene) Backbone and Cross-Conjugated Expanded Dendralenes. *Helv. Chim. Acta* **1995**, *78* (4), 779–796.

(56) Bryce, M. R.; Coffin, M. A.; Skabara, P. J.; Moore, A. J.; Batsanov, A. S.; Howard, J. A. K. Functionalised Oligoynes with Unusual Topologies: Synthesis, Electrochemistry and Structural Studies on Redox-Active [3]- and [4]-Dendralenes. *Chem. - Eur. J.* **2000**, *6* (11), 1955–1962.

(57) Zeng, Z.; Shi, X.; Chi, C.; López Navarrete, J. T.; Casado, J.; Wu, J. Pro-Aromatic and Anti-Aromatic π -Conjugated Molecules: An Irresistible Wish to Be Diradicals. *Chem. Soc. Rev.* **2015**, *44* (18), 6578–6596.

(58) Mishra, S.; Lohr, T. G.; Pignedoli, C. A.; Liu, J.; Berger, R.; Urgel, J. I.; Müllen, K.; Feng, X.; Ruffieux, P.; Fasel, R. Tailoring Bond Topologies in Open-Shell Graphene Nanostructures. *ACS Nano* **2018**, *12* (12), 11917–11927.

(59) Liu, J.; Mishra, S.; Pignedoli, C. A.; Passerone, D.; Urgel, J. I.; Fabrizio, A.; Lohr, T. G.; Ma, J.; Komber, H.; Baumgarten, M.; Corminboeuf, C.; Berger, R.; Ruffieux, P.; Müllen, K.; Fasel, R.; Feng, X. Open-Shell Nonbenzenoid Nanographenes Containing Two Pairs of Pentagonal and Heptagonal Rings. *J. Am. Chem. Soc.* **2019**, *141* (30), 12011–12020.

(60) Yang, S.; Olishchevski, P.; Kertesz, M. Bandgap Calculations for Conjugated Polymers. *Synth. Met.* **2004**, *141* (1–2), 171–177.

(61) Konishi, A.; Hirao, Y.; Nakano, M.; Shimizu, A.; Botek, E.; Champagne, B.; Shiomi, D.; Sato, K.; Takui, T.; Matsumoto, K.; Kurata, H.; Kubo, T. Synthesis and Characterization of Teranthene: A Singlet Biradical Polycyclic Aromatic Hydrocarbon Having Kekulé Structures. *J. Am. Chem. Soc.* **2010**, *132* (32), 11021–11023.

(62) Piquero-Zulaica, I.; Garcia-Lekue, A.; Colazzo, L.; Krug, C. K.; Mohammed, M. S. G.; Abd El-Fattah, Z. M.; Gottfried, J. M.; De Oteyza, D. G.; Ortega, J. E.; Lobo-Checa, J. Electronic Structure Tunability by Periodic Meta-Ligand Spacing in One-Dimensional Organic Semiconductors. *ACS Nano* **2018**, *12* (10), 10537–10544.

(63) Van der Veen, M. H.; Rispens, M. T.; Jonkman, H. T.; Hummelen, J. C. Molecules with Linear π -Conjugated Pathways between All Substituents: Omniconjugation. *Adv. Funct. Mater.* **2004**, *14* (3), 215–223.

(64) Sun, Q.; Gröning, O.; Overbeck, J.; Braun, O.; Perrin, M. L.; Borin Barin, G.; El Abbassi, M.; Eimre, K.; Dittler, E.; Daniels, C.; Meunier, V.; Pignedoli, C. A.; Calame, M.; Fasel, R.; Ruffieux, P. Massive Dirac Fermion Behavior in a Low Bandgap Graphene Nanoribbon Near a Topological Phase Boundary. *Adv. Mater.* **2020**, *32*, 1906054.

(65) Cirera, B.; Sánchez-Grande, A.; de la Torre, B.; Santos, J.; Edalatmanesh, S.; Rodríguez-Sánchez, E.; Lauwaet, K.; Mallada, B.; Zbořil, R.; Miranda, R.; Gröning, O.; Jelínek, P.; Martín, N.; Eciija, D. Tailoring Topological Order and π -Conjugation to Engineer Quasi-Metallic Polymers. *Nat. Nanotechnol.* **2020**, *15*, 437–443.

(66) Frisch, M. J.; Trucks, G. W.; Schlegel, H. B.; Scuseria, G. E.; Robb, M. A.; Cheeseman, J. R.; Scalmani, G.; Barone, V.; Petersson, G. A.; Nakatsuji, H.; Li, X.; Caricato, M.; Marenich, A. V.; Bloino, J.; Janesko, B. G.; Gomperts, R.; Mennucci, B.; Hratchian, H. P.; Ortiz, J. V.; Izmaylov, A. F.; et al. *Gaussian 16*, Rev. C.01; Gaussian: Wallingford, CT, USA, 2016.

(67) Zhao, Y.; Truhlar, D. G. The M06 Suite of Density Functionals for Main Group Thermochemistry, Thermochemical Kinetics, Noncovalent Interactions, Excited States, and Transition Elements: Two New Functionals and Systematic Testing of Four M06-Class Functionals and 12 Other Function. *Theor. Chem. Acc.* **2008**, *120*, 215–241.

(68) Dunning, T. H., Jr Gaussian Basis Sets for Use in Correlated Molecular Calculations. I. The Atoms Boron through Neon and Hydrogen. *J. Chem. Phys.* **1989**, *90* (2), 1007–1023.

(69) Krukau, A. V.; Vydrov, O. A.; Izmaylov, A. F.; Scuseria, G. E. Influence of the Exchange Screening Parameter on the Performance of Screened Hybrid Functionals. *J. Chem. Phys.* **2006**, *125* (22), 224106.

(70) Dennington, R.; Keith, T. A.; Millam, J. M. *GaussView*, Ver. 6.1; Semichem: Shawnee Mission, KS, USA, 2016.